Frontiers of Information Technology & Electronic Engineering
www.jzus.zju.edu.cn; engineering.cae.cn; www.springerlink.com
ISSN 2095-9184 (print); ISSN 2095-9230 (online)
E-mail: jzus@zju.edu.cn

2.3 μm nanosecond passive Q-switching of an LD-pumped Tm:YLF laser using gold nanorods as a saturable absorber*

Fu-yan WU, Shi-qiang WANG, Hai-wei CHEN, Hai-tao HUANG‡

School of Physics and Electronic Engineering, Jiangsu Normal University, Xuzhou 221116, China

E-mail: wfyjsnu@126.com; wsq274412@126.com; haiwei0819@163.com; hht840211@163.com

Received Mar. 13, 2020; Revision accepted May 5, 2020; Crosschecked June 5, 2020; Published online Sept. 14, 2020

Abstract: Developing new saturable absorbers for use in the mid-infrared region has practical significance for short-pulsed lasers and related scientific and industrial applications. The performance of gold nanorods (GNRs) as saturable absorbers at novel mid-infrared wavelengths needs to be evaluated even though these benefit from ultrafast nonlinear responses and broadband saturable absorption. Passive Q-switching of an LD-pumped 2.3 μm Tm:YLF laser using GNRs was successfully realized in this study. Pulses with an 843 ns pulse width and a 6.67 kHz repetition rate were achieved using this Q-switched laser. Results showed that GNRs provide promising passive Q-switches for 2.3 μm Tm-doped lasers.

Key words: Gold nanorods; Passive Q-switching; 2.3 μm; Tm-doped laser materials
https://doi.org/10.1631/FITEE.2000110 **CLC number:** TN248.1

1 Introduction

The output wavelengths of thulium lasers can cover a wide range from the near- to mid-infrared regions because of the abundant energy level structure of Tm^{3+} (Allain et al., 1989; Huang et al., 2017a; Wang H et al., 2017). The most popular laser transition, $^3F_4 \rightarrow {}^3H_6$, around 2 μm has been studied extensively and widely applied across many fields. Recently, however, another transition, $^3H_4 \rightarrow {}^3H_5$, has been shown to exhibit increasing potential for developing 2.3 μm thulium lasers (Guillemot et al., 2019, 2020; Morova et al., 2020; Muti et al., 2020). As the lower-level $^3H_5$ lies far away from the ground state $^3H_6$ (with energy greater than 8000 cm^{-1}), a 2.3 μm laser transition can be characterized as a four-level scheme. In contrast, a 2 μm laser transition faces the reabsorption effects induced by thermally populated ground level $^3H_6$. Thus, from an application perspective, a 2.3 μm laser is located within the strong absorption zone of CH_4, CO, and N_2O according to the HITRAN database. Biological tissue has a much weaker absorption in the 2.3 μm region than in the 2 μm region due to weak water absorption. This means that a 2.3 μm thulium laser using the $^3H_4 \rightarrow {}^3H_5$ transition has important potential applications in medical diagnosis and gas detection (McAleavey et al., 1997; Olesberg et al., 2005; Chao et al., 2013).

Note that 2.3 μm thulium lasers were initially focused on Yb and Tm co-doped materials (Diening et al., 1998). Thus, given about 976 nm laser diode (LD) pumping, the $^3H_4$ level of Tm^{3+} can be populated via a multistep energy transfer from Yb^{3+} to Tm^{3+}. This population process involves complex energy transfers and back transfer of Tm→Yb (Braud et al., 2000); however, Tm^{3+} single-doped materials can support a more efficient population mechanism

‡ Corresponding author

* Project supported by the National Natural Science Foundation of China (Nos. 61875077 and 61911530131) and the Natural Science Foundation of the Jiangsu Higher Education Institutions of China (No. 18KJA510001)

ORCID: Fu-yan WU, https://orcid.org/0000-0003-2755-1518; Hai-tao HUANG, https://orcid.org/0000-0002-2721-221X

(Sudesh and Piper, 2000). Upper-level $^3H_4$ can be populated by direct transition of $^3H_6 \rightarrow {}^3H_4$ with about 800 nm pumping. The laser performance of the $^3H_4 \rightarrow {}^3H_5$ transition in Tm:YLF lasers has been extensively studied; indeed, given a 780 nm Ti:sapphire laser for pumping, 200 mW continuous wave (CW) output power at 2.3 μm has been achieved (Pinto et al., 1994). One reason for choosing a 780 nm pumping wavelength is that it corresponds to the maximum peak of a π-polarized absorption spectrum of Tm:YLF. Research has also shown that a microsecond Q-switched 2309 nm Tm:YLF laser using Cr^{2+}:ZnSe can be realized, generating a 1.2 μs pulse width and 27 mW average output power (Canbaz et al., 2017a). Similarly, mode locking of a 2.3 μm Tm:YLF laser based on Kerr-lens and SESAM is realized with Ti:sapphire laser pumping (Canbaz et al., 2017a, 2017b; Soulard et al., 2017). Limitations of low output power and complex structure of a Ti:sapphire laser mean that a cost-effective, higher-output 2.3 μm Tm-doped laser should be explored. Commercially available AlGaAs LDs at 0.8 μm can easily be used to pump 2.3 μm Tm-doped lasers (Yorulmaz and Sennaroglu, 2018). We have recently developed an LD end-pumped Q-switched Tm:YLF laser using a $ReSe_2$-based saturable absorber (SA), outputting optimal pulse parameters of 486 mW, 716 ns, and 5.0 kHz (Wang SQ et al., 2019a). The 2.3 and 1.9 μm dual-wavelength Cr^{2+}:ZnSe-based Q-switching operation of a Tm:YLF laser was also achieved via 785 nm LD pumping (Huang et al., 2019).

Exploring new types of low-dimensional materials has practical significance for developing optoelectronic devices, including photodetectors, batteries, and short-pulsed lasers (Li PF et al., 2017; Song et al., 2017; Ge et al., 2018; Guo et al., 2018; Ji et al., 2018; Li ZJ et al., 2018; Ma et al., 2018; Wu et al., 2018; Xie et al., 2018, 2019a; Wang SQ et al., 2019b; Zhang et al., 2019). In this context, gold nanorods (GNRs) have become popular as nanomaterials because of their morphology-dependent anisotropic optical properties. Acting as saturated absorbers, GNRs have a number of clear comparative advantages. As a result of their surface plasmon resonance (SPR) effects, GNRs can introduce a strong electromagnetic field enhancement in the subwavelength local space, which greatly promotes interactions with light. The resultant low saturation strength is beneficial for realizing the low-threshold passive Q-switching operation. The saturable absorption effect of GNRs also has a wideband response ranging from the visible to mid-infrared, where the central SPR wavelength can be tuned by changing the size of GNRs. Plasmonic resonance is also polarization-dependent, related to GNR collective orientation. These nanorods are also easy to composite with other nanomaterials to realize the optimization of saturable absorber performance as well as the development of new functions (Xing et al., 2017; Xie et al., 2019b, 2020a, 2020b). GNRs have also been used successfully as SAs in near- to mid-infrared short-pulsed lasers (Huang et al., 2015; Luo et al., 2019; Qian et al., 2019). However, because of their ultrafast nonlinear optical responses and broadband SPR tunability, the Q-switching performance of GNRs SA at 2.3 μm remained unstudied.

GNRs were exploited as SA in this study to realize the 2.3 μm passive Q-switching of an LD-pumped Tm:YLF laser. Q-switched pulses with 843 ns pulse width, 6.67 kHz pulse repetition rate, and 320 mW average output power were obtained from this GNR-based pulsed laser.

2 Experimental setup

The sketch in Fig. 1 shows the LD end-pumped 2.3 μm Tm:YLF laser used in this analysis. The fiber-coupled CW LD pumping source had a central wavelength of 785 nm, while the core diameter and LD output fiber number aperture were set at 400 μm and 0.22 μm, respectively. A 1:1 optical collimator was used to couple LD radiation into the laser crystal. The input mirror M1 (plano-concave, 100 mm curvature radius) used for this experiment had antireflection coatings between 0.76 μm and 0.81 μm on one surface, while the other had high-reflection coatings between 2.25 μm and 2.38 μm as well as high-transmission coatings between 0.76 μm and 0.81 μm. The a-cut, 4 mm×4 mm×8 mm, 1.5 at. % Tm:YLF was placed in a water-cooling heat sink with the cooling temperature set at 18 °C. The Tm:YLF was antireflection-coated between 0.76 μm and 0.81 μm and between 2.25 μm and 2.38 μm on light-passing surfaces. The plane output coupler was partial-reflection coated with 1.5% transmissions between 2.25 μm and 2.38 μm on one surface and

antireflection-coated between 2.25 μm and 2.38 μm on the other. The physical length of the resonator was 30 mm.

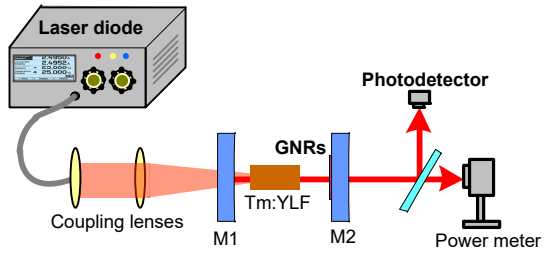

Fig. 1 Sketch of the LD-pumped Tm:YLF laser used in this analysis

3 Experimental results and discussion

At the point where the absorbed LD pump power attained 1.2 W, the Tm:YLF laser started to oscillate. The longer upper-level lifetime of 1.5 at. % Tm:YLF (0.86 ms) enabled the $^3H_4 \rightarrow {}^3H_5$ transition to achieve a low oscillation threshold. An optical spectrum analyzer (AQ6375, Yokogawa, Japan) was then used to record the laser spectrum (Fig. 2). Multiple wavelengths around 2306 nm were observed in the CW laser operation, which should be induced by the broadband fluorescence spectrum of $^3H_4 \rightarrow {}^3H_5$ transition in Tm:YLF. Variations in output power with absorbed LD pump power in the CW operation are shown in Fig. 3; when a maximum available absorbed LD pump power of 7.2 W was reached, 1.15 W output power was obtained.

GNRs were exploited as SA because of their significant Q-switching performance when used in a 2 μm thulium laser (Huang et al., 2016, 2017b). The average aspect ratio of GNRs (XFNANO) was 15; Fig. 4 presents the absorption spectrum measured using a spectrophotometer (Lambda 950, PerkinElmer, USA). Because of water absorption around 2 μm, the absorption spectrum of GNRs was measured with a non-solution-based sample (dry state). Absorption induced by the SPR of GNRs can be extended to the 2.3 μm region; thus, to minimize additional insertion loss, a GNR-based saturable output coupler (SOC) was also fabricated. The GNR-solution was drop-casted on the surface using 1.5% transmission coatings of the output coupler, and a room temperature slow-drying procedure was followed. The small-signal transmission of SOC at 2300 nm was measured to be about 0.8% while Q-switched pulses were captured with an oscilloscope (DPO7104C, Tektronix, USA) and a photodetector (Det10D, Thorlabs, USA).

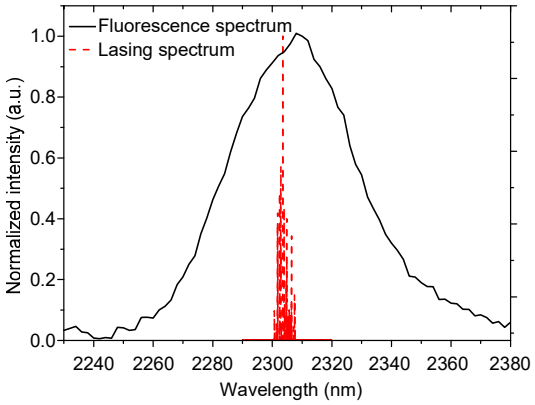

Fig. 2 Lasing spectrum of the LD-pumped Tm:YLF laser alongside the fluorescence spectrum

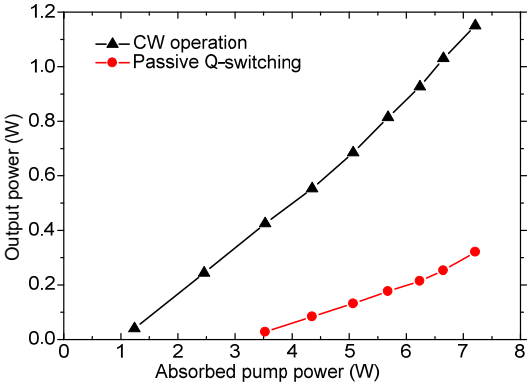

Fig. 3 Output power and absorbed LD pump power

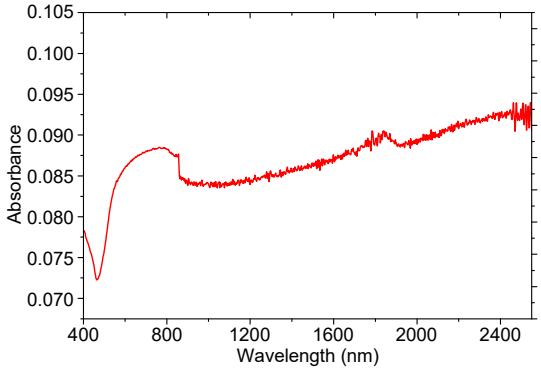

Fig. 4 Absorption spectrum of GNRs used in this experiment

The oscillation threshold for the GNR Q-switched laser was then raised to 3.5 W. A maximum average output power of 320 mW was achieved in this case, corresponding to an 8.6% slope efficiency. The ratio of the maximum output power in the passive Q-switching and continuous-wave case was 27.8%, and further spectral measurements showed that there was no difference in the output spectrum between Q-switching and the CW operation. The polarization states of the output laser beam in CW and passive Q-switching were measured as π-polarized.

The data presented in Fig. 5 showed the dependence of pulse characteristics (pulse repetition rate and pulse width) on absorbed LD pump power. A 2.25 μs pulse width and a 1.1 kHz pulse repetition rate were obtained slightly above the lasing threshold. Indeed, when the absorbed LD pump power was raised to 7.2 W, the pulse repetition rate was raised to 6.67 kHz, and the pulse width was narrowed to 843 ns. The data in Fig. 6 revealed the pulse shape with a minimum pulse width of 843 ns; in comparison with the 1.2 μs pulse width obtained in the Q-switched Tm:YLF/Cr:ZnSe laser (Canbaz et al., 2017a), the GNR Q-switched pulse achieved here was greatly reduced to the nanosecond region. It is clear that LD-pumped nanosecond 2.3 μm laser sources will have applications in pumping mid-infrared optical parametric oscillators.

4 Conclusions

The absorption spectrum of GNRs was extended to the 2.3 μm region using nanorods with a large aspect ratio. Passive Q-switching of an LD-pumped 2.3 μm Tm:YLF laser using GNRs as SA was demonstrated in this experiment. Nanosecond passive Q-switching operation using GNRs as SA was realized, generating pulses with optimal pulse parameters of 320 mW, 843 ns, and 6.67 kHz. The results of this analysis showed that GNRs provide promising passive Q-switches for 2.3 μm thulium lasers. In light of their broadband and smooth nonlinear absorption characteristics, GNR-based SAs have considerable potential in simultaneously generating multi-wavelength pulses from thulium lasers.

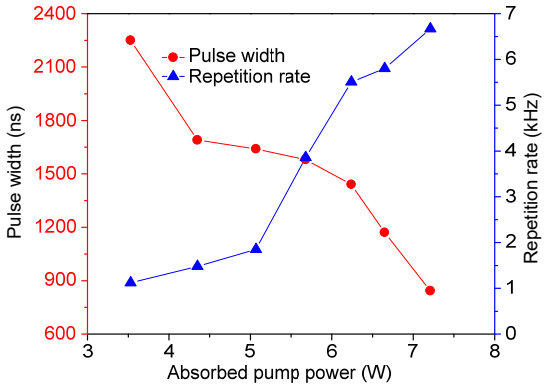

Fig. 5 Pulse characteristic dependence on absorbed LD pump power

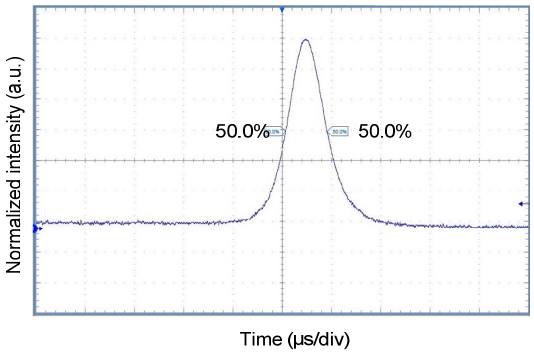

Fig. 6 Shape of the 843 ns pulse

Contributors

Hai-tao HUANG designed the research. Fu-yan WU and Shi-qiang WANG performed the experiment. Fu-yan WU drafted the manuscript. Hai-wei CHEN helped organize the manuscript. Hai-tao HUANG revised and finalized the paper.

Compliance with ethics guidelines

Fu-yan WU, Shi-qiang WANG, Hai-wei CHEN, and Hai-tao HUANG declare that they have no conflict of interest.

References

Allain JY, Monerie M, Poignant H, 1989. Tunable CW lasing around 0.82, 1.48, 1.88 and 2.35 μm in thulium-doped fluorozirconate fibre. *Electron Lett*, 25(24):1660-1662. https://doi.org/10.1049/el:19891113

Braud A, Girard S, Doualan JL, et al., 2000. Energy-transfer processes in Yb:Tm-doped KY_3F_{10}, $LiYF_4$, and BaY_2F_8 single crystals for laser operation at 1.5 and 2.3 μm. *Phys Rev B*, 61(8):5280-5292. https://doi.org/10.1103/PhysRevB.61.5280

Canbaz F, Yorulmaz I, Sennaroglu A, 2017a. 2.3-μm Tm^{3+}:YLF laser passively Q-switched with a Cr^{2+}:ZnSe saturable absorber. *Opt Lett*, 42(9):1656-1659. https://doi.org/10.1364/OL.42.001656

Canbaz F, Yorulmaz I, Sennaroglu A, 2017b. Kerr-lens

mode-locked 2.3-μm Tm^{3+}:YLF laser as a source of femtosecond pulses in the mid-infrared. *Opt Lett*, 42(19): 3964-3967. https://doi.org/10.1364/OL.42.003964

Chao X, Jeffries JB, Hanson RK, 2013. Real-time, in situ, continuous monitoring of CO in a pulverized-coal-fired power plant with a 2.3 μm laser absorption sensor. *Appl Phys B*, 110(3):359-365. https://doi.org/10.1007/s00340-012-5262-8

Diening A, Möbert PEA, Huber G, 1998. Diode-pumped continuous-wave, quasi-continuous-wave, and Q-switched laser operation of Yb^{3+},Tm^{3+}:$YLiF_4$ at 1.5 and 2.3 μm. *J Appl Phys*, 84(11):5900-5904. https://doi.org/10.1063/1.368876

Ge Y, Zhu Z, Xu Y, et al., 2018. Ultrafast photonics: broadband nonlinear photoresponse of 2D TiS_2 for ultrashort pulse generation and all-optical thresholding devices. *Adv Opt Mater*, 6:1870014. https://doi.org/10.1002/adom.201870014

Guillemot L, Loiko P, Braud A, et al., 2019. Continuous-wave Tm:$YAlO_3$ laser at ~2.3 μm. *Opt Lett*, 44(20):5077-5080. https://doi.org/10.1364/OL.44.005077

Guillemot L, Loiko P, Soulard R, et al., 2020. Close look on cubic Tm:KY_3F_{10} crystal for highly efficient lasing on the $^3H_4 \rightarrow {}^3H_5$ transition. *Opt Expr*, 28(3):3451-3463. https://doi.org/10.1364/OE.382650

Guo B, Wang SH, Wu ZX, et al., 2018. Sub-200 fs soliton mode-locked fiber laser based on bismuthene saturable absorber. *Opt Expr*, 26(18):22750-22760. https://doi.org/10.1364/OE.26.022750

Huang HT, Li M, Wang L, et al., 2015. Gold nanorods as single and combined saturable absorbers for a high-energy Q-switched Nd:YAG solid-state laser. *IEEE Photon J*, 7(4):4501210. https://doi.org/10.1109/JPHOT.2015.2460552

Huang HT, Li M, Liu P, et al., 2016. Gold nanorods as the saturable absorber for a diode-pumped nanosecond Q-switched 2 μm solid-state laser. *Opt Lett*, 41(12):2700-2703. https://doi.org/10.1364/OL.41.002700

Huang HT, Liu P, Liu X, et al., 2017a. Near-diffraction-limited diode end-pumped 2 μm Tm:YAG InnoSlab laser. *Laser Phys Lett*, 14(4):045805. https://doi.org/10.1088/1612-202X/aa5d82

Huang HT, Wang H, Shen DY, 2017b. VBG-locked continuous-wave and passively Q-switched Tm:Y_2O_3 ceramic laser at 2.1 μm. *Opt Mater Expr*, 7(9):3147-3154. https://doi.org/10.1364/OME.7.003147

Huang HT, Wang SQ, Chen HW, et al., 2019. High power simultaneous dual-wavelength CW and passively-Q-switched laser operation of LD pumped Tm:YLF at 1.9 and 2.3 μm. *Opt Expr*, 27(26):38593-38601. https://doi.org/10.1364/OE.381821

Ji XY, Kong N, Wang JQ, et al., 2018. A novel top-down synthesis of ultrathin 2D boron nanosheets for multimodal imaging-guided cancer therapy. *Adv Mater*, 30(36): 1803031. https://doi.org/10.1002/adma.201803031

Li PF, Chen Y, Yang TS, et al., 2017. Two-dimensional $CH_3NH_3PbI_3$ perovskite nanosheets for ultrafast pulsed fiber lasers. *ACS Appl Mater Interf*, 9(14):12759-12765. https://doi.org/10.1021/acsami.7b01709

Li ZJ, Qiao H, Guo ZN, et al., 2018. High-performance photoelectrochemical photodetector based on liquid-exfoliated few-layered InSe nanosheets with enhanced stability. *Adv Funct Mater*, 28(16):1705237. https://doi.org/10.1002/adfm.201705237

Luo HY, Kang Z, Gao Y, et al., 2019. Large aspect ratio gold nanorods (LAR-GNRs) for mid-infrared pulse generation with a tunable wavelength near 3 μm. *Opt Expr*, 27(4): 4886-4896. https://doi.org/10.1364/OE.27.004886

Ma DT, Li YL, Mi HW, et al., 2018. Robust SnO_{2-x} nanoparticle-impregnated carbon nanofibers with outstanding electrochemical performance for advanced sodium-ion batteries. *Angew Chem*, 130(29):9039-9043. https://doi.org/10.1002/ange.201802672

McAleavey FJ, O'Gorman J, Donegan JF, et al., 1997. Narrow linewidth, tunable Tm^{3+}-doped fluoride fiber laser for optical-based hydrocarbon gas sensing. *IEEE J Sel Top Quant Electron*, 3(4):1103-1111. https://doi.org/10.1109/2944.649549

Morova Y, Tonelli M, Petrov V, et al., 2020. Upconversion pumping of a 2.3 μm Tm^{3+}:KY_3F_{10} laser with a 1064 nm ytterbium fiber laser. *Opt Lett*, 45(4):931-934. https://doi.org/10.1364/OL.384284

Muti A, Canbaz F, Tonelli M, et al., 2020. Graphene mode-locked operation of Tm^{3+}:$YLiF_4$ and Tm^{3+}:KY_3F_{10} lasers near 2.3 μm. *Opt Lett*, 45(3):656-659. https://doi.org/10.1364/OL.385629

Olesberg JT, Arnold MA, Mermelstein C, et al., 2005. Tunable laser diode system for noninvasive blood glucose measurements. *Appl Spectrosc*, 59(12):1480-1484. https://doi.org/10.1366/000370205775142485

Pinto JF, Esterowitz L, Rosenblatt GH, 1994. Tm^{3+}:YLF laser continuously tunable between 2.20 and 2.46 μm. *Opt Lett*, 19(12):883-885. https://doi.org/10.1364/OL.19.000883

Qian QZ, Wang N, Zhao SZ, et al., 2019. Gold nanorods as saturable absorbers for the passively Q-switched Nd:LLF laser at 1.34 μm. *Chin Opt Lett*, 17(4):041401. https://doi.org/10.3788/COL201917.041401

Song YF, Liang ZM, Jiang XT, et al., 2017. Few-layer antimonene decorated microfiber: ultra-short pulse generation and all-optical thresholding with enhanced long term stability. *2D Mater*, 4(4):045010. https://doi.org/10.1088/2053-1583/aa87c1

Soulard R, Tyazhev A, Doualan JL, et al., 2017. 2.3 μm Tm^{3+}:YLF mode-locked laser. *Opt Lett*, 42(18):3534-3536. https://doi.org/10.1364/OL.42.003534

Sudesh V, Piper JA, 2000. Spectroscopy, modeling, and laser operation of thulium-doped crystals at 2.3 μm. *IEEE J Quant Electron*, 36(7):879-884. https://doi.org/10.1109/3.848362

Wang H, Huang HT, Liu P, et al., 2017. Diode-pumped continuous-wave and Q-switched Tm:Y_2O_3 ceramic laser around 2050 nm. *Opt Mater Expr*, 7(2):296-303.

https://doi.org/10.1364/OME.7.000296

Wang SQ, Huang HT, Chen HW, et al., 2019a. High efficiency nanosecond passively Q-switched 2.3 μm Tm:YLF laser using a $ReSe_2$-based saturable output coupler. *OSA Contin*, 2(5):1676-1682. https://doi.org/10.1364/OSAC.2.001676

Wang SQ, Huang HT, Liu X, et al., 2019b. Rhenium diselenide as the broadband saturable absorber for the nanosecond passively Q-switched thulium solid-state lasers. *Opt Mater*, 88:630-634. https://doi.org/10.1016/j.optmat.2018.12.042

Wu LM, Xie ZJ, Lu L, et al., 2018. Few-layer tin sulfide: a promising black-phosphorus-analogue 2D material with exceptionally large nonlinear optical response, high stability, and applications in all-optical switching and wavelength conversion. *Adv Opt Mater*, 6(2):1700985. https://doi.org/10.1002/adom.201700985

Xie ZJ, Xing CY, Huang WC, et al., 2018. Ultrathin 2D nonlayered tellurium nanosheets: facile liquid-phase exfoliation, characterization, and photoresponse with high performance and enhanced stability. *Adv Funct Mater*, 28(16):1705833. https://doi.org/10.1002/adfm.201705833

Xie ZJ, Chen SY, Duo YH, et al., 2019a. Biocompatible two-dimensional titanium nanosheets for multimodal imaging-guided cancer theranostics. *ACS Appl Mater Interf*, 11(25):22129-22140. https://doi.org/10.1021/acsami.9b04628

Xie ZJ, Zhang F, Liang ZM, et al., 2019b. Revealing of the ultrafast third-order nonlinear optical response and enabled photonic application in two-dimensional tin sulfide. *Photon Res*, 7(5):494-502. https://doi.org/10.1364/PRJ.7.000494

Xie ZJ, Duo YH, Lin ZT, et al., 2020a. The rise of 2D photothermal materials beyond graphene for clean water production. *Adv Sci*, 7(5):1902236. https://doi.org/10.1002/advs.201902236

Xie ZJ, Peng YP, Yu L, et al., 2020b. Solar-inspired water purification based on emerging 2D materials: status and challenges. *Sol RRL*, 4(3):1900400. https://doi.org/10.1002/solr.201900400

Xing CY, Xie ZJ, Liang ZM, et al., 2017. 2D nonlayered selenium nanosheets: facile synthesis, photoluminescence, and ultrafast photonics. *Adv Opt Mater*, 5(24):1700884. https://doi.org/10.1002/adom.201700884

Yorulmaz I, Sennaroglu A, 2018. Low-threshold diode pumped 2.3-μm Tm^{3+}:YLF lasers. *IEEE J Sel Top Quant Electron*, 24(5):1601007. https://doi.org/10.1109/JSTQE.2018.2791409

Zhang YP, Lim CK, Dai ZG, et al., 2019. Photonics and optoelectronics using nano-structured hybrid perovskite media and their optical cavities. *Phys Rep*, 795:1-51. https://doi.org/10.1016/j.physrep.2019.01.005